Dalton Transactions

Accepted Manuscript

ROYAL SOCIETY OF CHEMISTRY

www.rsc.org/dalton

Journal Name

ARTICLE

A series of dinuclear Dy(III) complexes bridged by 2-methyl-8-hydroxylquinoline: replacement on periphery coordinated β-diketonate terminal leads to different single-molecule magnetic properties

Received 00th January 20xx,
Accepted 00th January 20xx

DOI: 10.1039/x0xx00000x

www.rsc.org/

Wan-Ying Zhang,[a] Yong-Mei Tian,[a] Hong-Feng Li,[a] Peng Chen,[a] Wen-Bin Sun[a,*], Yi-Quan Zhang,[b,*] and Peng-Fei Yan[a,*]

A series of HMq-bridged dinuclear dysprosium complexes, namely, $[Dy(acac)_2(CH_3OH)]_2(\mu\text{-}HMq)_2$ (**1**), $[Dy(DBM)_2]_2(\mu\text{-}HMq)_2(n\text{-}C_6H_{14})$ (**2**), $[Dy(hmac)_2]_2(\mu\text{-}HMq)_2$ (**3**) and $[Dy(hfac)_3]_2(\mu\text{-}HMq)_2$ (**4**) (HMq = 2-methyl-8-hydroxyquinoline, acac = acetylacetone, DBM = dibenzoylmethane, hmac = hexamethylacetylacetonate and hfac = hexafluoroacetylacetonate), were structurally and magnetically characterized. X-ray crystallographic analysises of the structures reveal that HMq serves as the effective bridge to link two Dy(III) centers by means of the phenoxyl oxygen and nitrogen atoms and the periphery β-diketonate ligands complete the coordination sphere by bidentated oxygen atoms. The different substituents on the β-diketonate terminal lead to different coordination models mostly due to the steric hindrance of these substituents, and the electron-withdrawing or donating effects on which likely influenced the strength of ligand fields and the Dy(III) ion anisotropy. Measurements of alternating-current (ac) susceptibility on complexes **1**-**4** reveal that complexes **3** and **4** display significant zero-field single-molecule magnetic (SMM) behavior with barrier energy U_{eff}/k_B = 14.8 K, $\tau_0 = 1.8\times10^{-5}$ s and U_{eff}/k_B = 9.2 K, $\tau_0 = 1.7\times10^{-5}$ s, respectively, whereas **1** and **2** exhibit field-induced SMM behavior, and these differences are attributed to the alteration on the periphery β-diketonate ligands. Their distinct slow magnetic relaxation behaviors were related to their different individual Dy(III) ions magnetic anisotropy and intramolecular coupling, which were confirmed by ab initio calculation.

Introduction

There is currently high interest for the design of lanthanide complexes displaying single-molecule magnets (SMMs)[1] properties because of their wide variety of potential applications in molecular spintronics, ultrahigh density magnetic information storage and quantum computing.[2] Retrospectively, the synthesis and study of these pure 4f systems has literally been boosted since the discovery of prototype phthalocyanine sandwich complex $TbPc_2$ showing slow relaxation of the magnetization.[3] Most efforts have devoted to enhance the magnetization reversal, U_{eff}, and blocking temperatures, T_B, which are the major obstacle to realize the applications of SMMs. To this end, the high anisotropy of a molecule is generally expected. Indeed, the first unquenched orbital moment of some weighty lanthanides (Tb(III), Dy(III), Ho(III)) in association with the appropriate ligand field ultimately leads to high magnetic anisotropy.[4-9] The recent developments suggest that key factors in designing single-molecule magnets are maintaining rigorous axial symmetry within the molecule[10] or creating an exchange-bias through magnetic coupling. Exchange-biased systems resulting from magnetic coupling could provide the possibility to control the magnitude of the spin-reversal barrier as a function of the strength of the coupling.[11] They are highly promising to reduce the fast quantum tunnelling of magnetization (QTM) precluding the observation of a slow relaxation through the thermally activated barrier, and observe the enhanced performance SMMs. In view of this, the dinuclear SMMs systems obviously are supposed to be the ideal study platform and indeed the highest record of 14 K T_B was still kept by a dinuclear lanthanide complex featuring a N_2^{3-} radical-bridge that was found to be the hardest molecular magnet to date, $\{[((Me_3Si)_2N)_2Tb(THF)]_2(\mu\text{-}\eta^2\text{:}\eta^2\text{-}N_2)\}^{-}$.[12] Although introducing radical ligands has been proven successful in providing strong exchange interactions, such radicals are rarely found to directly bridge Ln(III) ions and are difficult to isolate. Only few

[a] Key Laboratory of Functional Inorganic Material Chemistry Ministry of Education, Heilongjiang University, Harbin 150080, P. R. China. E-mail: wenbinsun@126.com and yanpf@vip.sina.com
[b] Jiangsu Key Laboratory for NSLSCS, School of Physical Science and Technology, Nanjing Normal University, Nanjing 210023, P. R. China. E-mail: zhangyiquan@njnu.edu.cn

† Electronic Supplementary Information (ESI) available: Additional structural, magnetic data for the complexes. CCDC 1429731-1429734. For ESI and crystallographic data in CIF or other electronic format see DOI: 10.1039/x0xx00000x

examples are reported and consequently limit their exploration and further application.

8-Hydroxyquinoline (Hq) and its derivatives are versatile coordination ligands due to their flexible coordination modes of N and O atoms,[13] toward a wide range of metal ions, including lanthanide(III) ions. They exhibit versatile coordination modes including chelating, chelating-bridging in μ- and μ_3-phenoxo coordination modes, and bridging in μ-phenol modes.[14] In fact, after disclosure of electroluminescence properties of aluminum tris(8-quinolinolate) (Alq_3) and its successful application for fabrication of organic light-emitting devices,[15] lanthanide(III) complexes of 8-hydroxyquinolinates have been considered as one of most promising materials for the design of electroluminescent devices.[16] In contrast, these derivatives have sparsely been used as bridging ligand for modulation of lanthanide single-molecule magnet behavior.[17] Moreover, their successful fabrications on device are worthy learning for the further design of SMMs device, which promisingly furthers the prospects for realizing the application of single-molecule magnets.

In this paper, 2-methyl-8-hydroxyquinoline (HMq) is utilized to form series of dinuclear Dy(III) SMMs **1**-**4** by two modes (Scheme 1). One is μ-phenoxo mode, in which HMq serves as chelating-bridging ligand and the other is μ-phenol mode, and HMq serves as bridging ligand. In the four complexes, different periphery β-diketonate ligands coordinating to two Dy(III) ions dominate the final structures and their slow magnetic relaxation behaviors. We describe herein the preparation, structures and SMM properties of four lanthanide(III) complexes $[Dy(acac)_2(CH_3OH)]_2(\mu\text{-}HMq)_2$ (**1**), $[Dy(DBM)_2]_2(\mu\text{-}HMq)_2(n\text{-}C_6H_{14})$ (**2**), $[Dy(hmac)_2]_2(\mu\text{-}HMq)_2$ (**3**) and $[Dy(hfac)_3]_2(\mu\text{-}HMq)_2$ (**4**), where acac = acetylacetone, DBM = dibenzoylmethane, hmac = hexamethylacetylacetonate and hfac = hexafluoroacetylacetonate and the effects of these substituents on the β-diketonate terminal on the magnetic relaxations was discussed.

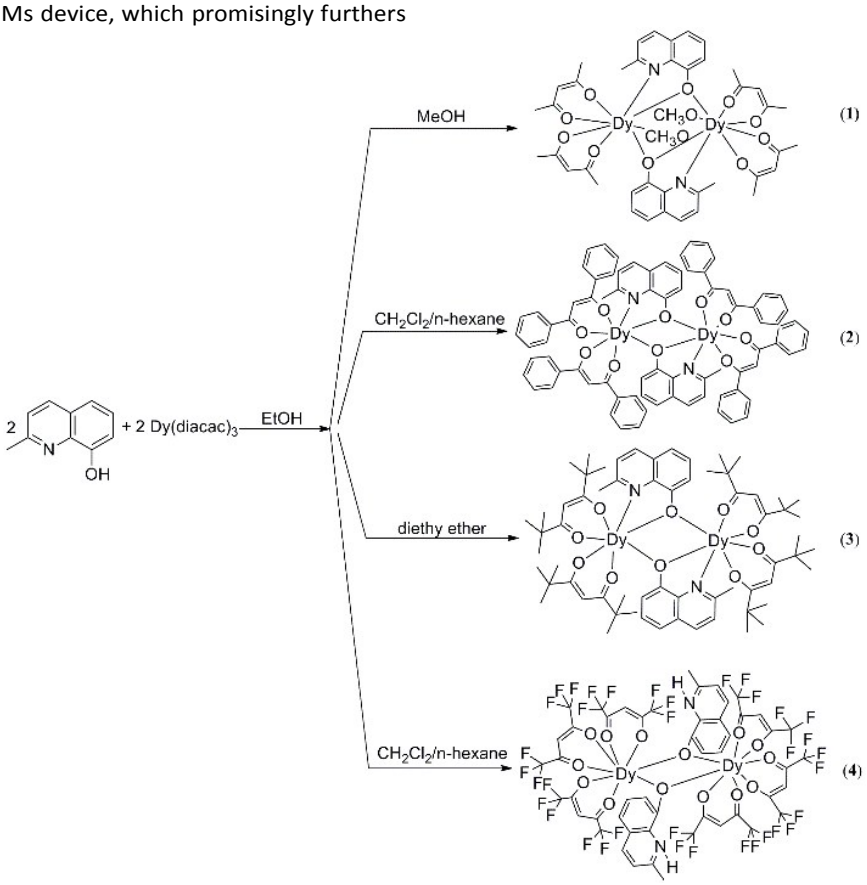

Scheme 1. The synthesis of complexes **1**-**4**.

Experimental Section

Materials and Methods. All chemicals and solvents were obtained from commercial sources and used as received without further purification. Elemental (C, H, and N) analyses were performed on a Perkin-Elmer 2400 analyzer. The magnetic susceptibilities of complexes **1**-**4** were measured using a Quantum Design VSM superconducting quantum interference device (SQUID) magnetometer. Data were corrected for the diamagnetism of the samples using Pascal constants and the sample holder by measurement. The lanthanide precursors, $LnL_3{\cdot}H_2O$ (L = β-diketonate ligands) were prepared according to the literature procedures previously described.[18] The construction of these four different complexes mainly thanks to the steric hindrance of methyl on the Mq backbone and the terminal β-diketonate ligands, but it

should be noticed that the solvent effects on the synthesis of these compounds should not be neglected.

*Synthesis of [Dy(acac)$_2$(CH$_3$OH)]$_2$(μ-Mq)$_2$ (**1**).* To a stirred solution of HMq (0.0796 g, 0.5 mmol) 10mL of EtOH, an ethyl alcohol solution (20 mL) of Dy(acac)$_3$·H$_2$O (0.240 g, 0.5 mmol) was added dropwise. The reaction mixture was refluxed and stirred for a further period of 6 h, resulting in a yellow precipitate. And then it was cooled and filtered, the coarse products were obtained as yellow sediments. They were dissolved in MeOH and kept for crystallization under slow evaporation conditions. After 3-4 days, pure rectangular-shaped yellow single crystals of complex **1** were obtained and collected. Yield: 0.198 g (72 %). Elemental analysis (%) calcd for $C_{42}H_{52}Dy_2N_2O_{12}$ (1101.86): C 45.74, H 4.72, N 2.54; found: C 45.69, H 4.61, N 2.43.

*Synthesis of [Dy(DBM)$_2$]$_2$(μ-HMq)$_2$(n-C$_6$H$_{14}$) (**2**).* To a stirred solution of HMq (0.0796 g, 0.5 mmol) 10mL of EtOH, an ethyl alcohol solution (20 mL) of Dy(DBM)$_3$·H$_2$O (0.426 g, 0.5 mmol) was added dropwise. The reaction mixture was refluxed and stirred for a further period of 6 h, resulting in a yellow precipitate. And then yellow coarse products were obtained after cooled and filtered. The final crystals were obtained by allowing hexane diffusing slowly into the dichloromethane solution of products in a sealed container after one week. Yield: 0.324 g (80 %). Elemental analysis (%) calcd for $C_{86}H_{74}Dy_2N_2O_{10}$ (1620.47): C 63.69, H 4.57, N 1.73; found: C 63.74, H 4.69, N 1.81.

*Synthesis of [Dy(hmac)$_2$]$_2$(μ-Mq)$_2$ (**3**).* A solution of Dy(hmac)$_3$ (0.356 g, 0.5 mmol) in EtOH (20 mL) was added dropwise to a solution of HMq (0.0796 g, 0.5 mmol) in EtOH (10 mL) and the mixture was stirred and refluxed for 6 h. Afterwards, the solution was cooled to room temperature and then the solvent was evaporated leading to a light yellow sediment. The light yellow products were isolated by recrystallization from diethyl ether. Yield: 0.289 g (84%). Elemental analysis (%) calcd for $C_{64}H_{92}Dy_2N_2O_{11}$ (1374.40): C 55.88, H 6.69, N 2.04; found: C 55.93, H 6.78, N 2.10.

*Synthesis of [Dy(hfac)$_3$]$_2$(μ-HMq)$_2$ (**4**).* A solution of Dy(hfac)$_3$·H$_2$O (0.401 g, 0.5 mmol) in EtOH (20 mL) was added dropwise to a solution of HMq (0.0796 g, 0.5 mmol) in EtOH (10 mL) and the mixture was stirred and refluxed for 6 h. Afterwards, the solution was cooled to room temperature and then the solvent was evaporated leading to a yellow sediment. The final crystals were obtained by allowing hexane diffusing slowly into the dichloromethane solution of product in a sealed container after one week. Yield: 0.387 g (82 %). Elemental analysis (%) calcd for $C_{50}H_{24}Dy_2F_{36}N_2O_{14}$ (1885.71): C 31.82, H 1.27, N 1.48; found: C 31.78, H 1.17, N 1.40.

*X-ray crystallographic Studies of **1**-**4**.* Crystal data for complexes **1**-**4** were collected on a Xcalibur, Eos, Gemini diffractometer with Mo Kα radiation (λ=0.71073 Å). All data were collected at a temperature of 293(2) K. The structures of complexes **1**-**4** were solved by direct methods and refined on F^2 by full-matrix least-squares using the SHELXTL-2014 program.[19] All non-hydrogen atoms were refined with isomorphous displacement parameters. For **2**, the hexane molecule has been modeled as disordered, however, the Ueq values are still relatively larger. The larger ellipsoid parameter might be owing to the thermal vibration of the hexane. For **3**, C21 C23 C29 C30 C31 C32 C33 C34 C41 C42 C43 C53 C54 C55 C56 C57 C58 C64 C65 C66 atoms have been modeled as disordered with equivalent occupancy. For **4**, the F atoms have been modeled as disordered with equivalent occupancy. The C-F distances in all the cases have been refined in the reasonable range. All crystallographic data for complexes **1**-**4** are summarized in Table 1, and selected bond lengths and angles for complexes **1**-**4** are tabulated in Table S1 (ESI†).

Table 1. Crystallographic details for complexes **1**-**4**.

	1	**2**	**3**	**4**
Empirical formula	$C_{42}H_{52}Dy_2N_2O_{12}$	$C_{86}H_{74}Dy_2N_2O_{10}$	$C_{64}H_{92}Dy_2N_2O_{10}$	$C_{50}H_{24}Dy_2F_{36}N_2O_{14}$
FW (g·mol^{-1})	1101.86	1620.47	1374.40	1885.71
Crystal system	Monoclinic	Triclinic	Monoclinic	Triclinic
Space group	*C*2/*c*	Pī	*P*2$_1$/*c*	Pī
Temperature (K)	293(2)	293(2)	293(2)	293(2)
a (Å)	24.6845(13)	13.0887 (8)	20.2210(5)	12.0760(6)
b (Å)	10.3099(4)	13.5801(8)	16.0209(4)	12.7204(6)
c (Å)	16.8554(7)	13.5961(7)	21.3696(5)	12.9553(6)
α (°)	90	102.811(5)	90	105.245(4)
β (°)	91.967(4)	112.601(5)	90.168(2)	112.104(4)
γ (°)	90	111.598(6)	90	106.283(4)
V (Å^3)	4287.1(3)	1876.6(3)	6922.8(3)	1610.82(17)
ρ_{cacd} (Mg·m^{-3})	1.707	1.387	1.320	1.944
μ (mm^{-1})	3.522	2.064	2.193	2.467
F(000)	2184	783	2812	906
Collected reflections	15912	15006	57671	13300
Independent relections	5129	8477	15487	7262
R_{int}	0.0445	0.0345	0.0375	0.0248
R_1 [I > 2σ(I)]	0.0285	0.0453	0.0552	0.0397
wR_2(all data)	0.0630	0.1219	0.1522	0.1043
GOF on F^2	1.114	1.125	1.090	1.047

a) $R_1 = \Sigma| |Fo| - |Fc||/\Sigma|Fo|$. b) $wR_2 = \Sigma[w(Fo^2 - Fc^2)^2] / \Sigma[w(Fo^2)^2]^{1/2}$.

Results and Discussion

Synthesis and Structures. The 8-Hydroxyquinoline-type lanthanide-based complexes exhibit versatile coordination modes including chelating, chelating-bridging in μ- and μ$_3$-phenoxo coordination modes, and bridging in μ-phenol modes, which strongly relies on the reaction condition such as lanthanide ionic radius, the nature of ancillary ligands and pH value of environment, even the subtle changes on the substituents of the ligand.[20] In order to investigate magnetic properties of 8-hydroxyquinoline-type dinuclear lanthanide-based complex, a derivative 2-methyl-8-hydroxyquinoline (HMq) was used, in which steric methyl on the Mq backbone serves to prevent formation of multinulcear lanthanide complexes and in combination with different β-diketonate ligands ultimately led to a variety of dinuclear lanthanide-based species. The crystal structure of **1** supported by the ancillary ligand acetylacetone, was depicted in Fig. 1.

Complex **1** crystallizes in the monoclinic space group *C*2/*c* (Table 1), as expected the central Dy atoms are bridged by two HMq ligands. The Dy(III) ion is coordinated by seven oxygen atoms with two from the μ-phenoxo of HMq, four from two acac$^-$, one from a coordinated MeOH, and one nitrogen atom from the μ-phenoxo of HMq, forming eight-coordinate environment. Therefore, the centrosymmetric dinuclear complex is composed of two eight-coordinated Dy(III) ions

bridged by phenoxo groups (O2, O2') of the HMq ligands with a Dy1-O2-Dy1' angle of 112.71(8)°, O2'-Dy1-O2 angle of 67.29(8)° and Dy-Dy distance equals to 3.9232(4) Å. The bond length of Dy1-O2 is 2.397(2) Å, and that of Dy1'-O2 is 2.316(2) Å. The shortest Dy···Dy distance between neighboring [DyDy] units is 9.6422(3) Å.

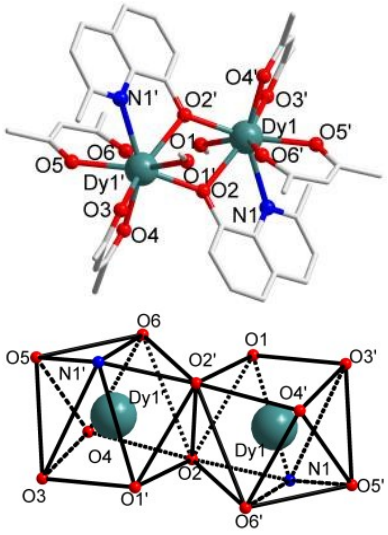

Fig. 1 The crystal structure of complex **1** (top) and local coordination geometry of the Dy(III) ions (bottom) (hydrogen atoms are omitted for clarity).

The local symmetry of the eight-coordinated structure was analysed by the continuous-shape measures (CShMs) method using the SHAPE software,[21] which allowed us to quantify the degree of distortion of the coordination sphere of real complexes (S value equals 0, corresponds to the perfect polyhedron). The relative large S values (Table S2†, ESI) indicate the coordination environment of the central Dy(III) ions in **1** is in a very low symmetry. Although they lie among the ideal hexagonal bipyramid (HBPY-8, D_{6h}), johnson gyrobifastigium J26 (JGBF-8, D_{2d}) and triakis tetrahedron (TT-8, T_d), respectively, but largely deviates the ideal polyhedron obviously with relative large S value 24.088, 24.917, and 26.928 respectively.

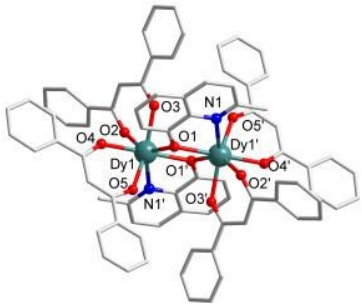

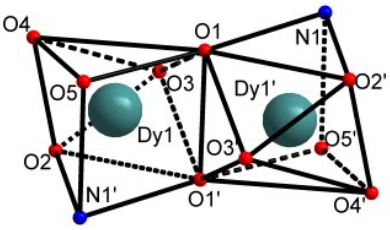

Fig. 2 The crystal structure of complex **2** (top) and local coordination geometry of the Dy(III) ions (bottom) (hydrogen atoms are omitted for clarity).

Generally, Ln(III) ions prefer high coordination numbers (8 or 9), in complex **1** the small size of acetylacetone cannot prevent a MeOH molecule squeezing into the coordination sphere of Dy(III) ions and leads to an overall NO7 coordination environment. Therefore, in order to protect Ln(III) ions from coordinating solvent molecules, other ancillary β-diketonate ligands with large steric hindrance should be used to form more stable and higher local symmetry complexes.

As expected, the complexes **2**-**4** were obtained without coordinating solvent molecules, which thanks to protection of larger steric hindrance of β-diketonate ligands i.e. dibenzoylmethane, hexamethylacetylacetonate and hexafluoroacetylacetonate respectively, their structures were depicted in Fig. 2-4.

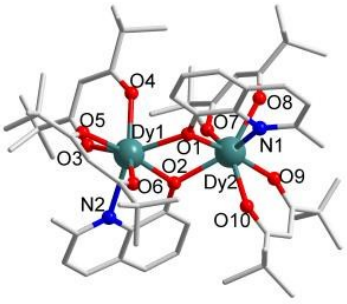

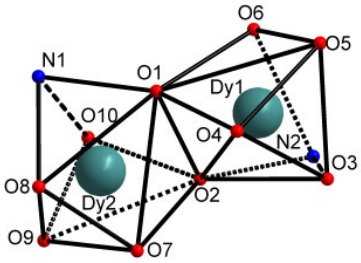

Fig. 3 The crystal structure of complex **3** (top) and local coordination geometry of the Dy(III) ions (bottom) (hydrogen atoms are omitted for clarity).

Although the complex **2** crystallized in the triclinic space group Pī (Table 1) and complex **3** crystallized in the monoclinic space group $P2_1/c$ (Table 1), the structural cores of complexes **2** and **3** are similar, differing only in the ancillary ligand β-diketonates (DBM and hmac). The central Dy(III) ions in complexes **2** and **3** are all seven-coordinated, one less than that of **1**, in which two oxygen atoms come from two HMq ligands, four oxygen atoms from two β-diketonates and one

nitrogen atom from the μ-phenoxo of HMq (Fig. 2-3). The bridging HMq is featured with a μ-phenoxo mode to link two Dy(III) ions in a symmetric fashion with the Dy-Dy distance being 3.7652(3) Å in complex **2** and an asymmetric fashion with the Dy-Dy distance being 3.7810(15) Å in complex **3**. Complex **2** has a Dy1-O1-Dy1' angle of 108.46(5)° and a O1-Dy1-O1' angle of 71.54(5)°. The Dy1-O1 and Dy1'-O1 distances are 2.3404(12) and 2.3001(13) Å, and the shortest Dy···Dy distance between neighboring [DyDy] units is 9.5840(5) Å. However, in complex **3**, the Dy1-O1-Dy2, O2-Dy1-O1, O1-Dy2-O2 and Dy1-O2-Dy2 angles are 109.57(5)°, 68.93(4)°, 69.08(4)° and 109.10(5)° and the Dy1-O1, Dy1-O2, Dy2-O1 and Dy2-O2 distances are 2.3322(13), 2.3070(14), 2.2955(14) and 2.3343(13) Å, respectively. The shortest Dy···Dy distance between neighboring [DyDy] units is 10.4286(2) Å.

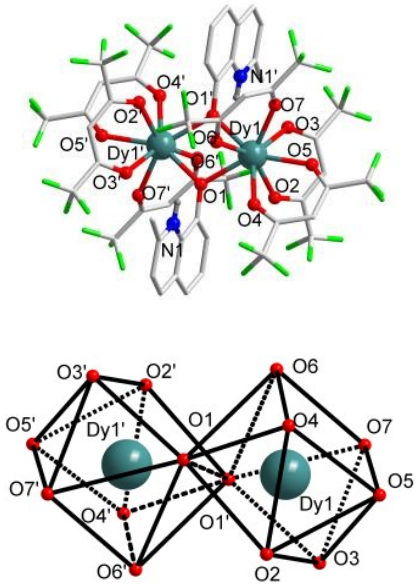

Fig. 4 The crystal structure of complex **4** (top) and local coordination geometry of the Dy(III) ions (bottom) (hydrogen atoms are omitted for clarity).

It is notable that the coordination environment in complexes **2** and **3** are similar but different from complex **4** (Fig. 4). Complex **4** crystallizes in the triclinic space group $P\bar{1}$ (Table 1). The Dy(III) ion is coordinated by eight oxygen atoms with two from the μ-phenoxo of HMq and six from three $hfac^-$, which without nitrogen atom from the μ-phenoxo of HMq, forming eight-coordinate environment. The bridging HMq is featured with a μ-phenol mode to link two Dy(III) ions in a symmetric fashion with the Dy-Dy distance being 3.8787(5) Å. The average bond length of the Dy–O is 2.360 Å, the Dy1-O1-Dy1' and O1-Dy1'-O1' angles are 110.75(11)° and 69.25(12)°. The shortest Dy···Dy distance between neighboring [DyDy] units is 10.0283(11) Å.

Through the above detailed structural parameters of the Dy(III) ion, it is noted that the distance between the centre of the Dy(III) ion is different for complexes **1**-**4**. The distance in complex **1** is the longest, that in complex **2** is the shortest and those in complexes **3** and **4** are medium. Moreover, the average Dy-O (β-diketonates) distances of **1**-**4** are 2.333 Å, 2.274 Å, 2.268 Å and 2.362 Å respectively.

The coordination geometries around Dy(III) ions in **2**-**4** are estimated by SHAPE software with the relative S values for complexes **2**-**4** summarizing in Table S2 (ESI†). The calculation indicates, for complexes **2** and **3**, the Dy(III) ions all lie among the ideal capped trigonal prism (CTPR-7, C_{2v}) and capped octahedron (COC-7, C_{3v}) with the S value of 2.798, 2.799 for complex **2** and 3.924, 4.280 for complex **3**. Moreover, coordination geometries of the Dy(III) ions in complex **4** are in a high geometrical symmetry showing square antiprism (SAPR-8, D_{4d}) with the S value 0.449 (Fig. 2-4). We notice that, among the complexes **1**-**4**, the S values of complexes **2** and **3** deviate less from an ideal C_{2v}-capped trigonal prism than the S value deviate from an ideal D_{6h}-hexagonal bipyramid which in complex **1**, and the S value of complex **4** deviating from an ideal D_{4d}-square antiprism is minimum. Obviously, complex **2** has higher coordination symmetry than that of complex **3**, and complex **4** has the highest coordination symmetry. All above significant disparities in **1**-**4** are mainly due to the different substituents on the β-diketonates terminal, which mostly likely lead to distinct magnetic behaviors.

Magnetic Properties. The direct current (dc) magnetic properties of complexes **1**-**4** were investigated under a 1000 Oe field in the temperature range 2-300 K (Fig. 5). Field dependence of the magnetization for complexes **1**-**4** between 2 and 8 K are shown in Fig. S1. At room temperature, the $\chi_M T$ values of complexes **1**-**4** are 28.5, 28.1, 28.9 and 28.9 $cm^3 \cdot K \cdot mol^{-1}$, respectively. These values are in good agreement with the expected theoretical values (28.34 $cm^3 \cdot K \cdot mol^{-1}$) for two free Dy(III) ions ($^6H_{15/2}$, S=5/2, L=5, g=4/3, C=14.17 $cm^3 \cdot K \cdot mol^{-1}$). On cooling, the $\chi_M T$ product of the complex steadily decreases down to 50 K during which the gradual drop in $\chi_M T$ is more pronounced for **1**, **2** than **3** and **4**. Below this temperature, there is a change of curvature and $\chi_M T$ decreases more abruptly, reaching a value of 21.53, 13.39, 11.71 and 13.39 $cm^3 \cdot K \cdot mol^{-1}$ at 2 K for **1**, **2**, **3** and **4** respectively. This behavior is due to the depopulation of the excited m_J sublevels of the Dy(III) ion, which arise from the splitting of the $^6H_{15/2}$ ground terms by the ligand field, and/or antiferromagnetic interactions between the Dy(III) centers. The M versus H plot for the Dy(III) complex shows a relatively rapid increase in the magnetization at low field to reach almost saturation for magnetic fields of 7 T. The observed saturation values for the Dy(III) complex are rather lower than the calculated ones, which is due to crystal-field effects leading to significant magnetic anisotropy and/or low-lying excited states.

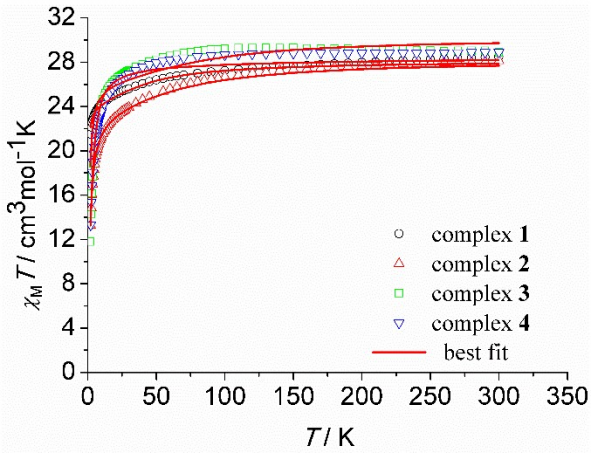

Fig. 5 Calculated (red solid line) and experimental data of magnetic susceptibility of complexes **1**-**4.**

In order to investigate the presence of slow relaxation of the magnetization which may originate from an SMM behavior, alternating-current (ac) measurements were performed on all complexes in the temperature range 2-20 K under zero dc field at frequencies between 1 and 1000 Hz. The temperature and frequency dependent ac susceptibility signals were observed below 10 K for the complexes **1**-**4** (Fig. 6-9 and Fig. S2–S5†, ESI).

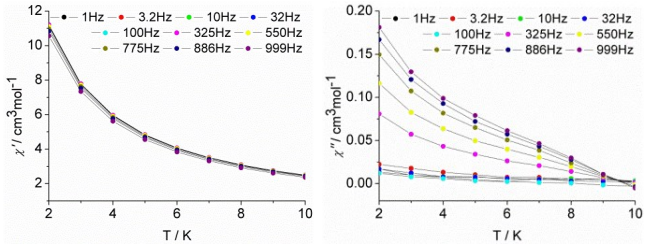

Fig. 6 Temperature dependence of the out-of-phase (χ'') ac susceptibility (left) and the in-phase (χ') ac susceptibility (right) in the frequency range 1-1000 Hz of complex **1** under 0 Oe.

The out-of-phase (χ'') susceptibilities show the frequency dependence behavior, which clearly indicates the slow relaxation of magnetization of **1**. In lanthanide SMMs systems, the tails of a peak generally indicate the presence of QTM, which reduces the expected thermally activated relaxation barrier. Owing to the Kramers nature of Dy(III) ion, at zero field, dipole–dipole and hyperfine interactions should be responsible for the mixing of the two Kramers ground states that allows the zero-field quantum tunneling dynamics of the magnetization. Therefore, the relaxation barriers cannot be extracted from this data as no full peak was observed in the absence of external field.

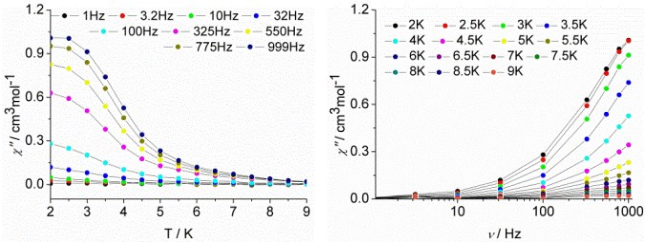

Fig. 7 Temperature dependence of the out-of-phase (χ'') ac susceptibility in the frequency range 1-1000 Hz (left) and frequency dependence of the out-of-phase (χ'') ac susceptibility in the temperature range 2-9 K (right) of complex **2** under 0 Oe.

However, the out-of-phase (χ'') susceptibilities of complexes **2**-**4** revealed the frequency dependence behavior between 1-1000 Hz and tending to a peak. Particularly, the clear peaks can be seen at frequencies higher than 550 Hz for complex **3** and the flat peaks can be seen in the pot of temperature dependent ac susceptibility, and full peaks can be observed in the pot of frequency dependent ac susceptibility for complex **4** (Fig. 7-9), meanwhile complex **2** shows only a poorly defined peak. This clearly indicates the SMM behaviors of complexes **2**-**4** are more significant than that of complex **1**.

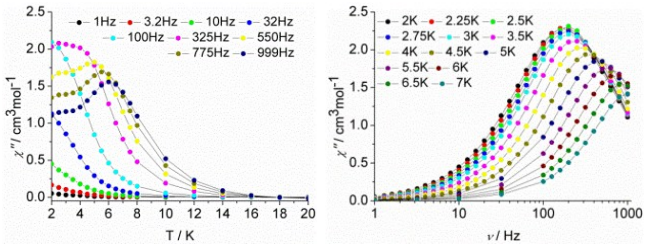

Fig. 8 Temperature dependence of the out-of-phase (χ'') ac susceptibility in the frequency range 1-1000 Hz (left) and frequency dependence of the out-of-phase (χ'') ac susceptibility in the temperature range 2-7 K (right) of complex **3** under 0 Oe.

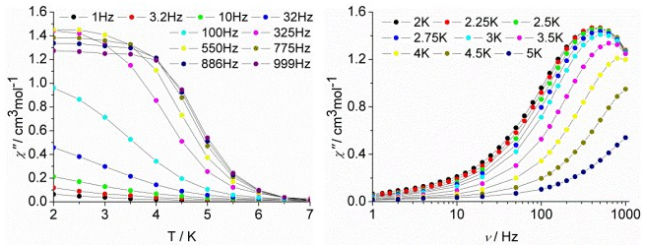

Fig. 9 Temperature dependence of the out-of-phase (χ'') ac susceptibility in the frequency range 1-1000 Hz (left) and frequency dependence of the out-of-phase (χ'') ac susceptibility in the temperature range 2-5 K (right) of complex **4** under 0 Oe.

It is possible to shortcut the QTM by applying a static dc field. Therefore, ac susceptibility measurements were performed under optimum static dc field of 2000, 1900, 1900 and 1500 Oe for complexes **1**-**4**, respectively (Fig. 10-13 and Fig. S6–S9†, ESI). The optimum field was selected by determining which field was able to slow the frequency dependent χ''

maxima to the slowest relaxation rate (Fig. S10-13†, ESI). As expected, after applying an external field the QTM was effectively suppressed and the full peaks of temperature dependence of ac susceptibility were observed. Similarly, the frequency-dependent data in the temperature range of 2–6 K display that the intensity of the χ'' increases with decreasing temperature and frequency (Fig. 10-13). This indicates slow relaxation of the magnetization associated with SMM behavior.

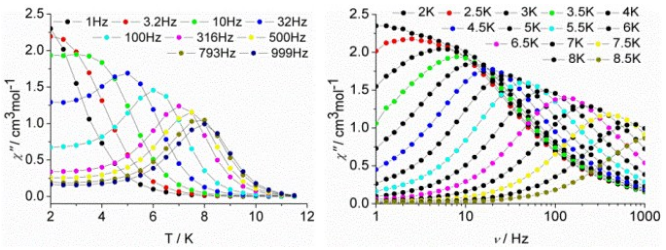

Fig. 10 Temperature dependence of the out-of-phase (χ'') ac susceptibility in the frequency range 1-1000 Hz (left) and frequency dependence of the out-of-phase (χ'') ac susceptibility in the temperature range 2-8.5 K (right) of complex **1** under 2000 Oe.

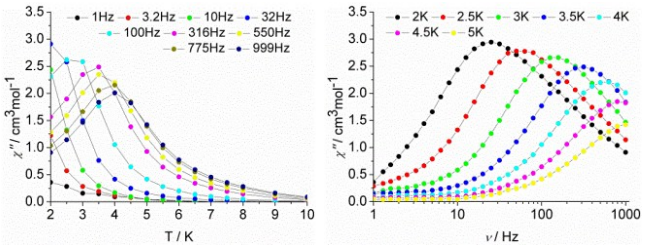

Fig. 11 Temperature dependence of the out-of-phase (χ'') ac susceptibility in the frequency range 1-1000 Hz (left) and frequency dependence of the out-of-phase (χ'') ac susceptibility in the temperature range 2-5 K (right) of complex **2** under 1900 Oe.

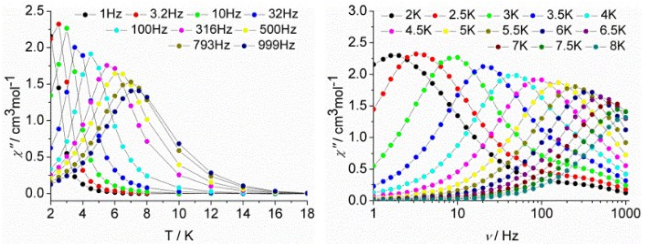

Fig. 12 Temperature dependence of the out-of-phase (χ'') ac susceptibility in the frequency range 1-1000 Hz (left) and frequency dependence of the out-of-phase (χ'') ac susceptibility in the temperature range 2-8 K (right) of complex **3** under 1900 Oe.

However, no matter the ac susceptibilities of complexes **1**-**4** were performed under zero dc field or an optimum dc field, the frequency dependence of the χ'' only displays mono peak which is likely indicative of a single thermally activated relaxations mechanism. For complexes **2** and **4**, the single relaxation mode in the frequency-dependent ac susceptibility is ascribed to the presence of a unique crystallographic Dy(III) ion in the triclinic space group P$\bar{1}$ system. Although complexes **1** and **3** have monoclinic crystal system, the visible single relaxation processes on the plot of the variation of χ'' versus the frequency were observed.

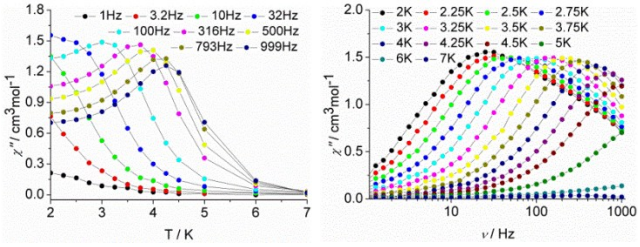

Fig. 13 Temperature dependence of the out-of-phase (χ'') ac susceptibility in the frequency range 1-1000 Hz (left) and frequency dependence of the out-of-phase (χ'') ac susceptibility in the temperature range 2-7 K (right) of complex **4** under 1500 Oe.

The graphical representation of χ'' vs χ' (Cole-Cole plot[22]) in a certain temperature range further confirms the single relaxation process. The data of complexes **3** and **4** can be fitted using a generalized Debye model[23] under zero dc field (Fig. S14-15† and Table S3-4†, ESI), and the date of complexes **1**-**4** be fitted under the optimum dc field (Fig. S16-19† and Table S5-8†, ESI). The parameter, indicating deviation from the pure Debye model, are in a range of 0.0–0.3 for these temperature range that increase significantly as the temperature decreases. These verify a single relaxation mode with a narrow distribution of relaxation times in complexes **1**-**4**.[24]

For a thermal assisted Orbach relaxation, magnetic data fitting to the high temperature linear regime using Arrhenius law ($\tau = \tau_0 \exp(U_{eff}/k_BT)$, Fig. 14) could provide an effective relaxation energy barrier U_{eff} and a pre-exponential factor τ_0. The curvature in the ln(τ) versus 1/T plot under zero field was observed for **3** and **4** and there is an apparent cross procedure from temperature-dependent regime associated with thermally active Orbach relaxation to a temperature independent regime related to the QTM upon lowering the temperature. In view of this, we fitted the magnetic data with the equation 1 considering the spin-lattice relaxation of both Orbach and QTM processes. The fitting results are collected in Table S9† (ESI).

$$1/\tau = 1/\tau_{QTM} + \tau_0^{-1}\exp(-U_{eff}/k_BT) \quad (1)$$

The high-temperature region (5-6.5 K for **3**, 3.5-4 K for **4**) was fitted using the pure Arrhenius law, which resulted in the estimated effective energy barrier to the magnetization reversal of U_{eff}/k_B = 14.8 K with $\tau_0 = 1.8\times10^{-5}$ s for **3** and U_{eff}/k_B = 9.2 K with $\tau_0 = 1.7\times10^{-5}$ s for **4** in the absence of dc field. The relaxation time of QTM for **3** and **4** are extracted from ac susceptibility as 0.8 ms and 0.3 ms, respectively.

To remove the QTM effect, the ac magnetic susceptibility measurements under applying an optimum field were performed for complexes **1**-**4**, respectively. It is also noteworthy that the plots of ln(τ) versus 1/T under an optimum field still exhibit obvious curvature which indicates

that perhaps another relaxation pathway is also operative (Fig. 14). The presence of multiple relaxation processes is possible as reported in a few SIMs.[25] In view of this, we fitted the magnetic data with the equation 2 considering the spin-lattice relaxation of both Raman and Orbach processes.[26]

$$1/\tau = CT^{n} + \tau_0^{-1}\exp(-U_{eff}/k_BT) \quad (2)$$

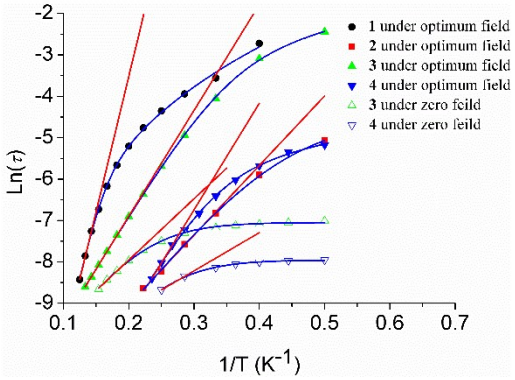

Fig. 14 Plot of ln(τ) versus 1/T at zero and optimum dc field for **1**-**4**. The blue lines represent the fitting of the frequency-dependent data by Equation 2 for **1**-**4** at optimum dc field and by Equation 1 for **3** and **4** at zero dc field. The red lines represent pure Arrhenius fitting at the high-temperature linear region for **1**-**4** at zero and optimum dc field.

The first and second terms correspond to the Raman and Orbach processes, respectively. In general, n = 9 is rational for Kramers ions, but when both the acoustic and optical phonons are considered depending on the structure of energy levels, n values between 1 and 6 are reasonable.[27] Equation 2 affords U_{eff}/k_B = 75.6 K, τ_0 = 2.1 ×10^{-8} s for complex **1** under 2000 Oe dc field, U_{eff}/k_B = 18.6 K, τ_0 = 2.9 ×10^{-6} s for complex **2** under 1900 Oe dc field, U_{eff}/k_B = 25.8 K, τ_0 = 6.1 ×10^{-6} s for complex **3** under 1900 Oe dc field, and U_{eff}/k_B = 26.9 K, τ_0 = 4.7 ×10^{-7} s for complex **4** under 1500 Oe dc field, respectively (see Fig. 14, Table S10†, ESI). Moreover, using the pure Arrhenius law to fit the high-temperature region (7-8 K for **1**, 3-4.5 K for **2**, 4.5-7.5 K for **3**, and 3.75-4.25 K for **4**) show that U_{eff}/k_B = 65.3 K, τ_0 = 6.3×10^{-8} s for complex **1**, U_{eff}/k_B = 16.8 K, τ_0 = 4.2×10^{-6} s for complex **2**, U_{eff}/k_B = 25.6 K, τ_0 = 6.1×10^{-6} s for complex **3** and U_{eff}/k_B = 25.7 K, τ_0 = 5.3×10^{-7} s for complex **4**, respectively under an optimum dc field (Fig. 14).

To further investigate magnetic anisotropy of dysprosium ions, ab initio calculation was used as an efficient and powerful method. Complete-active-space self-consistent field (CASSCF) calculations on two types of individual Dy(III) fragments for each of complexes **1–4** on the basis of X-ray determined geometries have been carried out with MOLCAS 7.8[28] and SINGLE_ANISO[29] programs (see Supporting Information for details). The lowest spin-orbit energies and the corresponding ***g*** tensors of complexes **1–4** are shown in Table S11† (ESI). From Table S11†, the calculated g_z values of the Dy(III) fragments of **1–3** are close to 20, which shows that the Dy(III)-Dy(III) exchange interactions for each of them can be approximately regarded as the Ising type. But, the Dy(III)-Dy(III) exchange interaction for **4** cannot be regarded as the Ising type due to its very small anisotropy of the Dy(III) fragment (see Table S11†). Moreover, the energy separations (Δ_{diff}) between the ground and the first Krammers doublets for the Dy(III) fragments of **1** and **4** are close to the fitting values extracted from the modified Arrhenius under optimum dc fields. However, the energy gaps in **2** and **3** are apparently deviated from the extracted experimental energy barriers. Normally, the Δ_{diff} is related with the thermally activated relaxation barrier through the first excited state i.e. Orbach machnism. Generally, the computed values are overestimating the U_{eff} values and the discrepancy between computed (U_{calcd}) and the experimental (U_{eff}) values are expected as the computed values assume inherently no QTM between the ground-state KDs and no intermolecular interactions or no vibronic coupling these are conditions that are very stringent and difficult to meet and not considered in the U_{calcd} values.[30]

The program POLY_ANISO[29] (see Figure 5) was used to fit the magnetic susceptibilities of complexes **1–4** using the exchange parameters from Table S12† (ESI).

All parameters for **1–3** from Table S12† were calculated with respect to the pseudospin $\tilde{S}$ = 1/2 of the Dy(III) ions. But, the *J* value of **4** in Table S12† was obtained with the spin of Dy(III) as 5/2. For four complexes, the total coupling parameters *J* (dipolar and exchange) were included into fit the magnetic susceptibilities. The calculated and experimental $\chi_M T$ versus *T* plots of complexes **1–4** are shown in Figure 5, where the fits are all close to the experimental data in the whole temperature regime.[31] From Table S12† (ESI), the Dy(III)-Dy(III) interactions of complexes **2** and **3** within Lines model[32] are both antiferromagnetic, but they are ferromagnetic for **1** and **4**. The main magnetic axes on two Dy(III) were indicated in Figure S20† (ESI), where the magnetic axes on the two Dy(III) ions for each complex have some differences (see Table S13†, ESI) . The strongest bonds between the metal center and the coordinated atoms may favor an axial nature of the ligand field and thus influences the single-ion anisotropy[33]. In this case, the easy axis in **1** and **4** are consistent with the bonds between metal center and the O atoms of β-diketonate ligands (Fig. S20† and Table S1†, ESI). However, the easy axes in **2** and **3** are approximately perpendicular to the plane formed by two oxygen atoms of HMq and two Dy(III) ions. The magnetization axes form angles of 46.42° and 31.11° with the Dy-Dy axes for **1** and **4**, and they are apparently smaller than the angle of 77.61° and 78.64° (81.24°) in **2** and **3**. In addition, MAGELLAN[34] was used to calculate the orientation of the anisotropy axes for each of the two Dy(III) ions in complexes **1**-**4** (Fig. S21† and Table S15†, ESI)**.** The results show that the orientations of magnetic anisotropy axes are roughly well predicted in complexes **1**-**3** with some deviations in contrast to those calculated by ab initio calculation. But, the deviation for **4** is relatively large (see Table S13† and S15†, ESI). These deviations are reasonable and mostly likely due to the MAGELLAN calculation is mainly based on a simple electrostatic method, neglects the intramolecular coupling and the environment beyond the first coordination sphere concerning only the coordinated atoms, or more precisely, the effective charges, and also neglects excited multiplets and inter-multiplet interactions.[35] Of course, it is very practical in determining of the orientation of the magnetic anisotropy of the pure $m_J = \pm^{15}/_2$ state of Dy(III).

We also gave the exchange energies and the main values of the g_z for the lowest two exchange doublets of four complexes in Table S14† (ESI) where the g_z values of the ground exchange states for **2** and **3** are both close to 0, which confirms that the Dy(III)-Dy(III) couplings are antiferromagnetic, but the g_z values of **1** and **4** are

nearly twice the g_z of the single Dy confirming the ferromagnetic Dy(III)-Dy(III) couplings. According to the ab initio results in combination with the experimental data of our case, which led us to the conclusion that the intramolecular coupling of Dy-Dy, ferro- or antiferromagnetic nature and their strength, are both important and apparent in determining their dynamic magnetic relaxation albeit relative weak. The antiferromagnetic interaction leads to a relative low energy barriers in **2** and **3** and contrarily complex **1** has the highest energy barrier (75.6 K) among them in which the g_z value of the ground exchange states is 39.2 (Table S14) which is indicative of nearly Ising type Dy(III)-Dy(III) interaction. Moreover, the anisotropy of individual Dy(III) is also important, for **4**, although the ferromagnetic interaction occurs, only a moderate energy barrier (26.9 K) is observed, which is most likely due to its small anisotropy of individual Dy(III) centers (Table S11) and vice versa, complex **3** have relative high individual anisotropy of Dy(III) (Table S11) while only small energy barrier 25.8 K was observed mainly due to the apparent antiferromagnetic interaction between Dy(III) ions. These results demonstrate that a joint contribution, combining single-ion anisotropy with strong magnetic coupling, may ultimately lead to higher relaxation barrier SMMs capable of retaining their magnetization at high practical temperatures.

Conclusions

A series of dinuclear Dy(III) SMMs were prepared as well as characterized structurally and magnetically. The structural analyses demonstrated that we successfully prevent the coordination of solvent molecules to Dy(III) ions utlizing the larger steric hindrance of ancillary ligand β-diketonates, and give rise to the low nuclearity Dy2 analogues with enhanced local symmetry. The distinct anisotropy axis of individual Dy(III) ions calculated by ab initio and MAGELLAN and the different anisotropy of individual Dy(III) ions and intramolecular couplings are most likely derived from the different substituents on the β-diketonate terminal, which ultimately leads to the significantly different SMM behaviors. The present work verifies that the sensitivity of magnetic relaxation to the remote alteration on individual spin centers, which provides an opportunity to shed light on tuning of the magnetic properties of SMMs.

Acknowledgements

This work was supported by the NSFC (no. 21572048, 21102039, 51302068, 21272061, 51102081, and 21302045), the Educational Commission of Heilongjiang Province (1254G045, 12541639), Natural Science Foundation of Jiangsu Province of China (BK20151542) and the Priority Academic Program Development of Jiangsu Higher Education Institutions.

Notes and references

1 (a) D. Gatteschi, R. Sessoli and J. Villain, Molecular Nanomagnets, Oxford University Press, 2006; (b) T. Glaser, *Chem. Commun.*, 2011, **47**, 116; (c) R. A. Layfield, *Organometallics*, 2014, **33**, 1084.

2 (a) D. Gatteschi, A. Caneschi, L. Pardi and R. Sessoli, *Science*, 1994, **265**, 1054; (b) M. Yamanouchi, D. Chiba, F. Matsukura and H. Ohno, *Nature*, 2004, **428**, 539; (c) R. Bagai and G. Christou, *Chem. Soc. Rev.*, 2009, **38**, 1011; (d) D. N. Woodruff, R. E. Winpenny and R. A. Layfield, *Chem. Rev.*, 2013, **113**, 5110.

3 (a) R. Sessoli and A. K. Powell, *Coord. Chem. Rev.*, 2009, **253**, 2328; (b) F. Habib and M. Murugesu, *Chem. Soc. Rev.*, 2013, **42**, 3278; (c) L. Sorace, C. Benelli and D. Gatteschi, *Chem. Soc. Rev.*, 2011, **40**, 3092; (d) N. Ishikawa, M. Sugita, T. Ishikawa, S. Y. Koshihara and Y. Kaizu, *J. Am. Chem. Soc.*, 2003, **125**, 8694.

4 (a) P. Zhang, Y.-N. Guo and J. Tang, *Coord. Chem. Rev.*, 2013, **257**, 1728; (b) H. L. C. Feltham and S. Brooker, *Coord. Chem. Rev.*, 2014, **276**, 1; (c) Y.-N. Guo, G.-F. Xu, Y. Gao and J. Tang, *Dalton Trans.*, 2011, **40**, 9953.

5 (a) S. Yamauchi, T. Fujinami, N. Matsumoto, N. Mochida, T. Ishida, Y. Sunatsuki, M. Watanabe, M. Tsuchimoto, C. Coletti and N. Re, *Inorg. Chem.*, 2014, **53**, 5961; (b) S. K. Langley, N. F. Chilton, B. Moubaraki and K. S. Murray, *Chem. Commun.*, 2013, **49**, 6965; (c) V. E. Campbell, R. Guillot, E. Riviere, P.-T. Brun, W. Wernsdorfer and T. Mallah, *Inorg. Chem.*, 2013, **52**, 5194.

6 (a) S. Demir, J. M. Zadrozny and J. R. Long, *Chem. -Eur. J.*, 2014, **20**, 9524; (b) L. Ungur, J. J. Le Roy, I. Korobkov, M. Murugesu and L. F. Chibotaru, *Angew. Chem., Int. Ed.*, 2014, **53**, 4413; (c) M.-E. Boulon, G. Cucinotta, S.-S. Liu, S.-D. Jiang, L. Ungur, L. F. Chibotaru, S. Gao and R. Sessoli, *Chem. -Eur. J.*, 2013, **19**, 13726.

7 (a) N. Ishikawa, M. Sugita, T. Ishikawa, S.-Y. Koshihara and Y. Kaizu, *J. Phys. Chem. B*, 2004, **108**, 11265; (b) C. R. Ganivet, B. Ballesteros, G. de la Torre, J. M. Clemente-Juan, E. Coronado and T. Torres, *Chem. -Eur. J.*, 2013, **19**, 1457.

8 (a) K. Yamashita, R. Miyazaki, Y. Kataoka, T. Nakanishi, Y. Hasegawa, M. Nakano, T. Yamamura and T. Kajiwara, *Dalton Trans.*, 2013, **42**, 1987; (b) M. Maeda, S. Hino, K. Yamashita, Y. Kataoka, M. Nakano, T. Yamamura and T. Kajiwara, *Dalton Trans.*, 2012, **41**, 13640.

9 J. Ruiz, A. J. Mota, A. Rodríguez-Diéguez, S. Titos, J. M. Herrera, E. Ruiz, E. Cremades, J. P. Costes and E. Colacio, *Chem. Commun.*, 2012, **48**, 7916.

10 (a) C. Gorller-Walrand, K. Binnemans, K. A. Gschneidner and L. Eyring, Handbook on the Physics and Chemistry of Rare Earths, 1996, **23**; (b) N. Ishikawa, M. Sugita and W. Wernsdorfer, *Angew. Chem., Int. Ed.*, 2005, **44**, 2931; (c) S. Takamatsu, T. Ishikawa, S. Y. Koshihara and N. Ishikawa, *Inorg. Chem.*, 2007, **46**, 7250; (d) J. L. Liu, Y. C. Chen, Y. Z. Zheng, W. Q. Lin, L. Ungur, W. Wernsdorfer, L. F. Chibotaru and M. L. Tong, *Chem. Sci.*, 2013, **4**, 3310.

11 (a) F. Habib, P.-H. Lin, J. Long, I. Korobkov, W. Wernsdorfer and M. Murugesu, *J. Am. Chem. Soc.*, 2011, **133**, 8830; (b) S.-F. Xue, Y.-N. Guo, L. Ungur, J.-K. Tang and L. F. Chibotaru, *Chem.-Eur. J.*, 2015, **21**, 1; (c) J. J. Le Roy, L. Ungur, I. Korobkov, L. F. Chibotaru and M. Murugesu, *J. Am. Chem. Soc.*, 2014, **136**, 8003.

12 J. D. Rinehart, M. Fang, W. J. Evans and J. R. Long, *J. Am. Chem. Soc.*, 2011, **133**, 14236.

13 C. W. Tang and S. A. VanSlyke, *Appl. Phys. Lett.*, 1987, **51**, 913.

14 (a) R. Van Deun, P. Fias, P. Nockemann, A. Schepers, T. N. Parac-Vogt, K. Van Hecke, L. vanMeervelt and K. Binnemans, *Inorg. Chem.*, 2004, **43**, 8461; (b) H.-B. Xu, H.-M.Wen, Z.-H. Chen, J. Li, L.-X. Shi and Z.-N. Chen, *Dalton Trans.*, 2010, **39**, 1948; (c) H. He, X. Zhu, A. Hou, J. Guo, W.-K. Wong, W.-Y. Wong, K.-F. Li and K.-W. Cheah, *Dalton Trans.*, 2004, 4064.

15 T. Sano, Y. Nishio, Y. Hamada, H. Takahashi, T. Usuki and K. Shibata, *J. Mater. Chem.*, 2000, **10**, 157.
16 (a) M. Albrecht, R. Frohlich, J.-C. G. Bünzli, A. Aebischer, F. Gumy and J. Hamacek, *J. Am. Chem. Soc.*, 2007, **129**, 14178; (b) R. Kikkeri, L. H. Hossain and P. H. Seeberger, *Chem. Commun.*, 2008, 2127; (c) S. Comby, D. Imbert, C. Vandevyver and J.-C. G. Bunzli, *Chem.-Eur. J.*, 2007, **13**, 936.
17 (a) E. M. Pineda, N. F. Chilton, R. Marx, María Dörfel, D. O. Sells, P. Neugebauer, S.-D. Jiang, D. Collison, J. van Slageren, E. J.L. McInnes and R. E.P. Winpenny, *Nat. Commun.*, 2014, **5**, 5243; (b) N. F. Chilton, G. B. Deacon, O. Gazukin, P. C. Junk, B. Kersting, S. K. Langley, B. Moubaraki, K. S. Murray, F. Schleife, M. Shome, D. R. Turner and J. A. Walker, *Inorg. Chem.*, 2014, **53**, 2528; (c) W. M. Wang, H. X. Zhang, S. Y. Wang, H. Y. Shen, H. L. Gao, J. Z. Cui and B. Zhao, *Inorg. Chem.*, 2015, **54**, 10610; (d) L. Zhang, P. Zhang, L. Zhao, J. F. Wu, M. Guo and T. K. Tang, *Inorg. Chem.*, 2015, **54**, 5571; (e) H. X. Zhang, S. Y. Wang, W. M. Wang, H. L. Gao and J. Z. Cui, *Inorg. Chem. Commun.*, 2015, **62**, 94.
18 (a) Y. Hasegawa, Y. Kimura, K. Murakoshi, Y. Wada, J.-H. Kim, N. Nakashima, T. Yamanaka and S. J. Yanagida, *Phys. Chem.*, 1996, **100**, 10201; (b) H. Bauer, J. Blanc and D. L. Ross, *J. Am. Chem. Soc.*, 1964, **86**, 5125.
19 G. M. Sheldrick, *Acta Cryst*. *C*, 2015, **71**, 3−8.
20 H.-B. Xu, J. Li, L.-X. Shi and Z.-N. Chen, *Dalton Trans.*, 2010, **40**, 5549.
21 M. Llunell, D. Casanova, J. Cirera, P. Alemany, S. Alvarez, SHAPE, v2.1; University of Barcelona and The Hebrew University of Jerusalem, Barcelona and Jerusalem, 2013.
22 (a) K. S. Cole and R. H. J. Cole, *Chem. Soc.*, 1941, **9**, 341; (b) S. M. J. Aubin, Z. Sun, L. Pardi, J. Krzystek, K. Folting, L. J. Brunel, A. L. Rheingold, G. Christou and D. N. Hendrickson, *Inorg. Chem.*, 1999, **38**, 5329.
23 D. Gatteschi, R. Sessoli and J. Villain, Molecular Nanomagnets, Oxford University Press: New York, 2006 and references therein.
24 J. Long, F. Habib, P.-H. Lin, I. Korobkov, G. Enright, L. Ungur, W. Wernsdorfer, L. F. Chibotaru and M. Murugesu, *J. Am. Chem. Soc.*, 2011, **133**, 5319.
25 (a) S. Titos-Padilla, J. Ruiz, J. M. Herrera, E. K. Brechin, W. Wersndorfer, F. Lloret, E. *Colacio, Inorg. Chem.*, 2013, **52**, 9620; (b) J. L. Liu, K. Yuan, J. D. Leng, L. Ungur, W. Wernsdorfer, F. S. Guo, L. F. Chibotaru, M. L. Tong, *Inorg. Chem.*, 2012, **51**, 8538; (c) E. Colacio, J. Ruiz, E. Ruiz, E. Cremades, J. Krzystek, S. Carretta, J. Cano, T. Guidi, W. Wernsdorfer, E. K. Brechin, *Angew. Chem. Int. Ed.*, 2013, **52**, 9130; (d) W.-B. Sun, B. Yan, Y.-Q. Zhang, B.-W. Wang, Z.-M. Wang, J.-H. Jia, S. Gao, *Inorg. Chem. Front.*, 2014, **1**, 503; (e) W. B. Sun, P. F. Yan, Sh. D. Jiang, B. W. Wang, Y. Q. Zhang, H. Fe. Li, P. Chen, Z. M. Wang, S. Gao, *Chem. Sci.*, 2016, **7**, 684.
26 A. Abragam, B. Bleaney, Electron Paramagnetic Resonance of Transition Ions; Clarendon Press: Oxford, U.K., 1970.
27 K. N. Shirivastava, *Phys. Status Solidi B*, 1983, **117**, 437.
28 G. Karlström, R. Lindh, P. -Å. Malmqvist, B. O. Roos, U. Ryde, V. Veryazov, P. -O. Widmark, M. Cossi, B. Schimmelpfennig, P. Neogrady and L. Seijo, MOLCAS: a Program Package for Computational Chemistry. *Comput. Mater. Sci*. 2003, **28**, 222.
29 (a) L. F. Chibotaru, L. Ungur and A. Soncini, *Angew. Chem. Int. Ed.*, 2008, **47**, 4126. (b) L. Ungur, W. Van den Heuvel and L. F. Chibotaru, *New J. Chem.*, 2009, **33**, 1224. (c) L. F. Chibotaru, L. Ungur, C. Aronica, H. Elmoll, G. Pilet and D. Luneau, *J. Am. Chem. Soc.*, 2008, **130**, 12445.
30 (a) L. Ungur, L. F. Chibotaru, *Phys. Chem. Chem. Phy.*, 2011, **13**, 20086; (b) D. Aravena, E. Ruiz, *Inorg. Chem.*, 2013, **52**, 13770; (c) J. M. Zadrozny, M. Atanasov, A. M. Bryan, C. Y. Lin, B. D. Rekken, P. P. Power, F. Neese, J. R. Long, *Chem. Sci.*, 2013, **4**, 125; (d) M. Atanasov, J. M. Zadrozny, J. R. Long, F. Neese, *Chem. Sci.*, 2013, **4**, 139.
31 S. K. Langley, D. P. Wielechowski, V. Vieru, N. F. Chilton, B. Moubaraki, B. F. Abrahams, L. F. Chibotaru and K. S. Murray, *Angew. Chem. Int. Ed*., 2013, **52**, 12014.
32 M. E. Lines, *J. Chem. Phys*., 1971, **55**, 2977.
33 S. F. Xue, Y. N. Guo, L. Ungur, J. K. Tang, L. F. Chibotaru, *Chem. Eur. J.*, 2015, **21**, 14099.
34 N. F. Chilton, D. Collison, E. J.L. McInnes, R. E.P. Winpenny and A. Soncini, *Nat. Commun.*, 2013, **4**, 2551.
35 K. Qian, J. J. Baldoví, S.-D. Jiang, A. Gaita-Ariño, Y.-Q. Zhang, J. Overgaard, B.-W. Wang, E. Coronado and S. Gao, *Chem. Sci.*, 2015, **6**, 4587.